Journal of Computational and Applied Mathematics 11 (1984) 11–25
North-Holland

Finite element formulation of thermal boundary layers

Nader ZAMANI
Centre for Computer Aided Design, Technical University of Nova Scotia, Halifax, Nova Scotia, Canada

Farhad NAFEIY
Department of Engineering Economic Systems, Stanford University, Palo Alto, CA, U.S.A.

Received 25 August 1983
Revised 24 January 1984

Abstract: In this article we discuss the finite element discretization of the two-dimensional, incompressible, and turbulent boundary layers. The formulation of the momentum equation is essentially due to Baker and Soliman [1] with some modifications.

The versatility and the accuracy of the method is established by considering several test cases. The predictions are satisfactory and compare favorably with alternative numerical techniques.

Keywords: Finite element method, thermal boundary layers, turbulence.

1. Introduction

The objective of this article is to discuss the finite element formulation of two-dimensional thermal boundary layers. It is assumed that the flow is steady, incompressible, and that the surface curvature effect is negligible. Problems of this nature are very common is aerodynamics and convective heat transfer.

The domain of the solution of the governing equations is a finite or semi-infinite region which originates at a suitable point on the surface. The choice of this point and more information on the geometry of the problem are discussed in the later sections.

In order to handle turbulence, a simple Prandtl's mixing length model due to Van Driest [15] is employed which has produced good results. More sophisticated models, e.g., turbulent kinetic energy and viscous dissipation can be used but only at the expense of solving two more equations. For details on turbulence modelling we refer to [8].

In the finite element discretization, only linear shape functions are used but the extension to higher-order functions is obvious. The governing equations in the boundary layers are nonlinear and parabolic. Therefore, results from the one-dimensional non-steady heat conduction can serve as guidelines in the course of computation. In particular, Crank–Nicolson type averaging is introduced and some of the stability results are heuristically investigated.

Due to the incompressibility assumption, the momentum and energy equations are decoupled

and each is solved independently of the other. To be more specific, the momentum equation is first considered and then the energy equation is solved. Due to the nonlinearity of the governing equations, iterative numerical process is the only choice.

Prior to the development of high-speed computers, the most popular techniques for solving boundary layer equations were the integral methods and the series solutions. However, in the past two decades, the trend has considerably changed and more emphasis is placed on the direct solution of the governing partial differential equations. This trend is reflected in [1,2,3,5,6,9,11]. The present formulation follows the development in [1].

2. Description of the geometry

As mentioned before, the two-dimensional boundary layer equations are usually solved in a finite or a semi-infinite region. This region is bounded by the solid surface on the one hand and the 99% boundary layer thickness on the other. The thickness grows in the downstream direction and it has to be calculated and adjusted as the marching is performed (see Fig. 1(a)).

The initial point x_0 which determines the left-hand boundary is selected at a position where accurate information on the velocity profile can be obtained. If the fluid separates from the wall, the right-hand boundary is fixed at the point of separation. The same situation arises where the surface comes to an end prior to separation. This again results in a finite region. Otherwise, the domain of the differential equation is a semi-infinite region.

To give concrete examples, for uniform flow past a circular cylinder the domain is finite due to separation. On the other hand, for uniform flow past a long flat plate, the domain is semi-infinite. In Fig. 1(a), a bounded domain is depicted.

3. The governing equations

The boundary layer equations for two-dimensional, steady, turbulent, and incompressible flow with negligible surface curvature effects are given by

$$u\frac{\partial u}{\partial x}+v\frac{\partial u}{\partial y}-\frac{\partial}{\partial y}\left((\nu_l+\nu_t)\frac{\partial u}{\partial y}\right)-u_p\frac{du_p}{dx}=0 \quad \text{momentum},$$

$$u\frac{\partial T}{\partial x}+v\frac{\partial T}{\partial y}-\frac{1}{\rho c}\frac{\partial}{\partial y}\left((k_l+k_t)\frac{\partial T}{\partial y}\right)=0 \quad \text{energy},$$

$$\frac{\partial u}{\partial x}+\frac{\partial v}{\partial y}=0 \quad \text{continuity}.$$

The coordinates x and y are measured along the surface and normal to it starting at an arbitrary

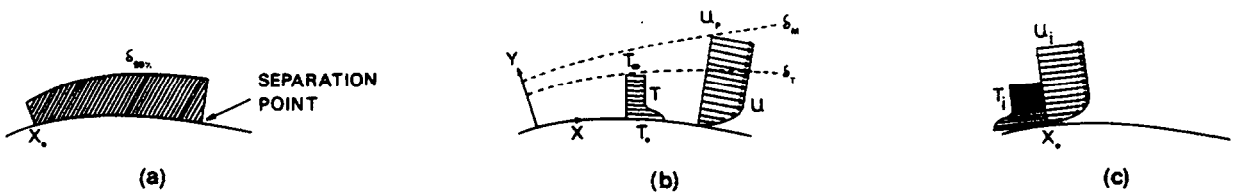

Fig. 1.

point x_0. Variables u and v are the velocities in the x and y directions respectively, and finally, T is the temperature profile (see Fig. 1(b)).

The initial and boundary conditions associated with the above differential equations are listed below.

$$
\begin{aligned}
&u(x,0)=v(x,0)=0 && \text{no slip,}\\
&u(x,\delta_{\mathrm{M}})=u_p(x) && \text{free stream,}\\
&u(x_0,y)=u_{\mathrm{i}}(y) && \text{initial velocity distribution,}\\
&T(x,0)=T_0 && \text{surface temperature,}\\
&T(x,\delta_{\mathrm{T}})=T_\infty && \text{free stream temperature,}\\
&T(x_0,y)=T_{\mathrm{i}}(y) && \text{initial temperature distribution.}
\end{aligned}
$$

Here, T_0 and T_∞ are the surface and free stream temperatures, u_p is the potential flow velocity at the edge of the boundary layer and δ_{M} is the 99% boundary layer thickness. δ_{T} is the corresponding thermal boundary layer thickness.

In fluid mechanics, it is convenient to nondimensionalize the equations. One possibility is the following change of variables

$$
\bar{x}=\frac{x}{L},\qquad \bar{y}=\frac{y\sqrt{\mathrm{Re}}}{L},\qquad \bar{u}_p=\frac{u_p}{U_\infty\sqrt{\mathrm{Re}}},
$$

$$
\bar{u}=\frac{u}{U_\infty\sqrt{\mathrm{Re}}},\qquad \bar{v}=\frac{v}{U_\infty},\qquad \bar{T}=\frac{T-T_0}{T_\infty-T_0},
$$

where Re denotes the Reynolds number. In the new coordinate system (after dropping the bars for simplicity) the governing equations are

$$
\begin{aligned}
&u\frac{\partial u}{\partial x}+v\frac{\partial u}{\partial y}-\frac{1}{\sqrt{\mathrm{Re}}}\frac{\partial}{\partial y}\left(\left(1+\frac{\nu_{\mathrm{t}}}{\nu_{\mathrm{l}}}\right)\frac{\partial u}{\partial y}\right)-u_p\frac{\mathrm{d}u_p}{\mathrm{d}x}=0 && \text{momentum,}\\
&u\frac{\partial T}{\partial x}+v\frac{\partial T}{\partial y}-\frac{1}{\mathrm{Pr}\sqrt{\mathrm{Re}}}\frac{\partial}{\partial y}\left(\left(1+\frac{k_{\mathrm{t}}}{k_{\mathrm{l}}}\right)\frac{\partial T}{\partial y}\right)=0 && \text{energy,}\\
&\frac{\partial u}{\partial x}+\frac{\partial v}{\partial y}=0 && \text{continuity.}
\end{aligned}
$$

The initial and boundary conditions now appear as

$$
\begin{aligned}
&u(x,0)=v(x,0)=0 && \text{no slip,}\\
&u(x,\delta_{\mathrm{M}})=u_p/\left(U_\infty\sqrt{\mathrm{Re}}\right) && \text{free stream,}\\
&u(x_0,y)=u_{\mathrm{i}}/\left(U_\infty\sqrt{\mathrm{Re}}\right) && \text{initial velocity distribution,}\\
&T(x,0)=0 && \text{surface temperature,}\\
&T(x,\delta_{\mathrm{T}})=1 && \text{free stream temperature,}\\
&T(x_0,y)=\left(T_{\mathrm{i}}(y)-T_0\right)/(T_\infty-T_0) && \text{initial temperature distribution.}
\end{aligned}
$$

The constant Pr appearing in the transformed energy equation is the Prandtl number.

4. Notation

The notation used in this paper is summarized below for easy reference.

x, y	streamwise and transverse directions,
x_0, L	x-coordinate of the initial point and characteristic length,
u, v	streamwise and transverse velocities,
u_i, T_i	initial velocity and temperature profiles,
u_p, p	potential flow velocity and the corresponding pressure,
U_∞	free stream velocity,
T	temperature distribution within the boundary layer,
T_0, T_∞	surface and free stream temperatures,
δ_M, δ_T	99% momentum and thermal boundary layer thicknesses,
ρ	density,
ν_l, ν_t	kinematic and eddy viscosities,
k_l, k_t	thermal and eddy conductivities,
c	specific heat,
α	thermal diffusivity,
τ_w, q_w	shear stress and heat flux at the wall,
Re	$= U_\infty L/\nu_l$, Reynolds number based on L and U_∞,
Pr	$= \nu_l/\alpha$, Prandtl number,
Nu_x	$= xq_w/(k_l(T_0 - T_\infty))$, local Nusselt number,
St_x	$= \alpha \mathrm{Nu}_x/U_\infty$, local Stanton number,
cf_x	$= \tau_w/(0.5\, u_p^2)$, local friction coefficient.

5. Turbulene model

An elementary way to specify turbulence model is Prandtl mixing length theory. The formulation below is due to Cebeci [5].

$$\nu_t = \begin{cases} (\nu_t)_i = l^2 \dfrac{\partial u}{\partial y} & \text{the inner region,} \\ (\nu_t)_o = 0.0168\, \delta^* & \text{the outer region,} \end{cases}$$

where

$$u_\tau = \sqrt{\frac{\tau_w}{\rho}}, \qquad p^+ = \frac{\nu_l u_p}{u_\tau^3} \frac{\mathrm{d}u_p}{\mathrm{d}x}, \qquad N = (1 - 11.8\, p^+)^{1/2},$$

$$A = 26 \cdot \frac{\nu_l}{N u_\tau}, \qquad l = 0.4\, y(1 - \mathrm{e}^{-y/A}) \quad \text{mixing length.}$$

The calculation of ν_t requires some explanation. Given a velocity profile u, one has to calculate $(\nu_t)_o$. Then starting at the wall, $(\nu_t)_i$ is computed in the transverse direction. At some point, $(\nu_t)_i$ exceeds $(\nu_t)_o$. This point is taken as the boundary of the inner and outer regions.

The turbulent Prandtl number $\mathrm{Pr}_t = \mu_t c/k_t$ is taken to be the constant 0.9. This practice is

recommended by Browne [4]. Thus k_t, the turbulent eddy conductivity is calculated according to

$$k_t = \nu_t \frac{\rho c}{0.9}.$$

Now that ν_t and k_t are unambiguously defined, the finite element method can be applied.

6. Finite element formulation

6.1. Momentum equation

At each x-station, a grid across the boundary layer is constructed, see Fig. 2(a). Within each element $(i, i+1)$, the variables u, v, and ν_t are assumed to vary linearly according to

$$u = N_1 u_1 + N_2 u_2, \qquad v = N_1 v_1 + N_2 v_2, \qquad \nu_t = N_1 \nu_{t1} + N_2 \nu_{t2}.$$

Here the subscripts refer to the local lable of the nodes and the shape functions N_1 and N_2 are expressed in local coordinate system as in Fig. 3. The nodal degrees of freedom u_1, u_2, v_1, v_2, ν_{t1} and ν_{t2} are functions of x only. The momentum equation is required to be satisfied locally, i.e.,

$$\int_{y_{i+1}}^{y_i} \left[u\frac{\partial u}{\partial x} + v\frac{\partial u}{\partial y} - \frac{1}{\sqrt{\mathrm{Re}}}\frac{\partial}{\partial y}\left(\left(1+\frac{\nu_t}{\nu_1}\right)\frac{\partial u}{\partial y}\right) - u_p\frac{\mathrm{d}u_p}{\mathrm{d}x}\right] N_j(y)\,\mathrm{d}y = 0, \quad j = 1, 2.$$

After some algebraic manipulations, integration by parts leads to the following matrix differential

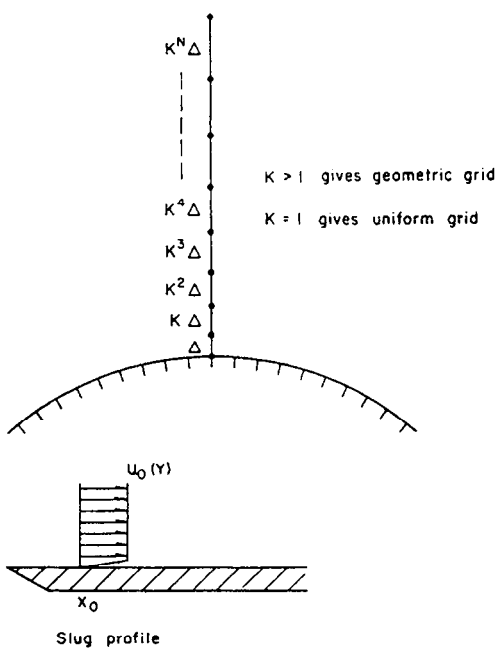

Fig. 2.

$$S = \frac{Y - Y_{j+1}}{\Delta e}$$

Fig. 3.

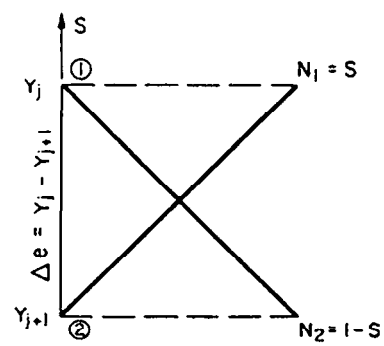

equation

$$K(U)\dot{U} + [G(V) + H(\nu)]U + S = 0, \tag{6.1}$$

where

$$U = [u_1, u_2]^T, \qquad \dot{U} = \left[\frac{du_1}{dx}, \frac{du_2}{dx}\right]^T, \qquad V = [v_1, v_2]^T, \qquad \nu_t = [\nu_{t1}, \nu_{t2}]^T,$$

$$K(U) = \tfrac{1}{12}\Delta y \left[\begin{array}{c|c} 3u_1 + u_2 & u_1 + u_2 \\ \hline u_1 + u_2 & u_1 + 3u_2 \end{array}\right], \qquad G(V) = \tfrac{1}{6}\left[\begin{array}{c|c} 2v_1 + v_2 & -2v_1 - v_2 \\ \hline v_1 + 2v_2 & -v_1 - 2v_2 \end{array}\right],$$

$$H(\nu) = \frac{1}{2\nu_l \Delta y \sqrt{\mathrm{Re}}}\left[\begin{array}{c|c} 2\nu_l + \nu_{t1} + \nu_{t2} & -2\nu_l - \nu_{t1} - \nu_{t2} \\ \hline -2\nu_l - \nu_{t1} - \nu_{t2} & 2\nu_l + \nu_{t1} + \nu_{t2} \end{array}\right], \qquad S = -\tfrac{1}{2}\Delta y\, u_p \frac{du_p}{dx}[1, 1]^T.$$

The system of ODEs (6.1) is now discretized using a combination of the backward Euler scheme and the Crank–Nicolson type averaging in the following manner:

$$K(U^{n+1})\frac{U^{n+1} - U^n}{\Delta x} + [G(V^n) + H(\nu^n)][\lambda U^{n+1} + (1 - \lambda)U^n] + S = 0. \tag{6.2}$$

The parameter λ controls the degree of implicitness in (6.2) and plays an important role in the stability of calculations. Notice that v_1, v_2, ν_{t1} and ν_{t2} are substituted from the station x_n. The result is a system of nonlinear algebraic equations involving $U^{n+1} = [u_1^{n+1}, u_2^{n+1}]^T$. The Newton–Raphson iteration algorithm is employed for the purpose of linearization.

To start the iteration process, the velocity profile $U^n = [u_1^n, u_2^n]^T$ from the previous x-station is used. The expression (6.2) is for a single element, therefore, the assembly step is followed.

Due to the linearity of the shape functions, the global Jacobian matrix is tridiagonal and the solution can be obtained by Thomas' algorithm. Once the u velocities are computed satisfactorily, the integrated version of the continuity equation can be employed to obtain the v component, namely

$$v(y) = -\int_0^y \frac{\partial u(x, s)}{\partial x} ds.$$

6.2. Energy equation

Now that the velocity fields at x_{n+1} are available, the temperature nodal values can be calculated. Within the element $(i, i + 1)$, the variables u, v, k_t and T are expressed as

$$u = N_1 u_1 + N_2 u_2, \qquad v = N_1 v_1 + N_2 v_2, \qquad k_t = N_1 k_{t1} + N_2 k_{t2}, \qquad T = N_1 T_1 + N_2 T_2.$$

Again u_i, v_i, k_{ti} and T_i, $i = 1, 2$, are functions of x only. The energy equation is forced to be satisfied locally and this is achieved by

$$\int_{y_{i-1}}^{y_i} \left[u\frac{\partial T}{\partial x} + v\frac{\partial T}{\partial y} - \frac{1}{\mathrm{Pr}\sqrt{\mathrm{Re}}}\frac{\partial}{\partial y}\left(\left(1 + \frac{k_t}{k_l}\right)\frac{\partial T}{\partial y}\right)\right] N_j(y)\, dy = 0, \quad j = 1, 2. \tag{6.3}$$

As in the momentum equation, after algebraic manipulations and integration by parts, the following matrix differential equation is obtained:

$$K(U)\dot{T} + [G(V) + L(k_t)]T = 0. \tag{6.4}$$

Here, K and G are the 2×2 matrices defined previously whereas T, $\dot{T}$ and L are given below

$$T = [T_1, T_2]^{\mathrm{T}}, \qquad \dot{T} = \left[\frac{\mathrm{d}T_1}{\mathrm{d}x}, \frac{\mathrm{d}T_2}{\mathrm{d}x}\right]^{\mathrm{T}},$$

$$L(k_t) = \frac{1}{2k_1 \operatorname{Pr}\sqrt{\operatorname{Re}}} \left[\begin{array}{c|c} 2k_1 + k_{t1} + k_{t2} & -2k_1 - k_{t1} - k_{t2} \\ \hline -2k_1 - k_{t1} - k_{t2} & 2k_1 + k_{t1} + k_{t2} \end{array}\right], \quad k_t = [k_{t1}, k_{t2}]^{\mathrm{T}}.$$

The backward Euler scheme is used for discretization of (6.4). The result is expressed by

$$K(U^{n+1})\frac{T^{n+1} - T^n}{\Delta x} + \left[G(V^{n+1}) + L\left(k_t^{n+1}\right)\right]T^{n+1} = 0. \tag{6.5}$$

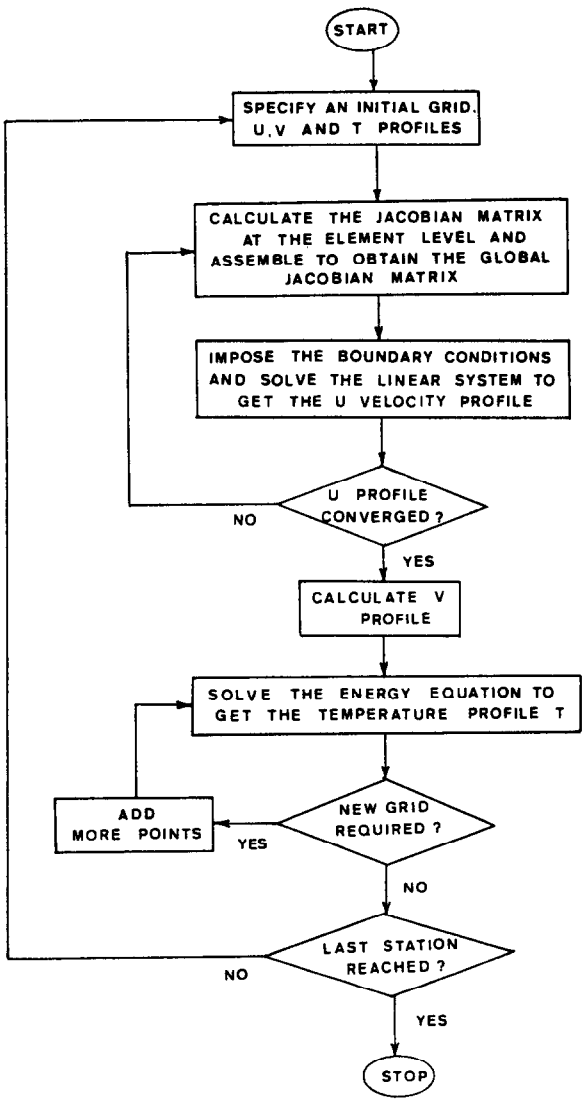

Fig. 4.

In the above expression, k_i^{n+1} is known by virtue of its definition in Section 5. Clearly (6.5) is linear in terms of T^{n+1} and consequently the assembly process results in a tridiagonal system of linear equations in terms of T^{n+1}. The overall sequence of calculations is shown in the flow chart of Fig. 4.

7. Selection of x_0 and the initial conditions

Due to the parabolic nature of the boundary layer equations, $u_i(y)$, the initial velocity profile and $T_i(y)$ the initial temperature distribution at x_0 must be specified.

The point x_0 itself must be selected so that $u_i(y)$ and $T_i(y)$ can accurately be described. Therefore, the critical quantities are $u_i(y)$ and $T_i(y)$. One possibility is the experimental values at a particular point. Although such information is highly desirable, it may not always be available. In some cases, the exact similarity solutions in the laminar regime can be used to simulate the initial data (see, e.g., the laminar flow over a flat plate, Section 10).

In many instances, a slug profile, Fig. 2(b), is sufficient for a reasonable initial data. The only constraint on such a profile is the requirement that its slope at the wall be consistent with the shear stress or the heat flux at the same point.

In our calculations, the initial v profile is set identically equal to zero. This practice does not pose a serious problem for two reasons. First, it is well known that in the boundary layer region, $v \ll u$ holds. Secondly, only after a few stations (typically 2 or 3), the v component approaches its true nonzero value.

8. Geometric grid and grid growth

In the case of laminar flow, a uniform grid in the y direction is sufficient for computational purposes. However, in turbulent flow the situation is different. Many researchers have recommended the use of the so called geometric grids as shown in Fig. 2(a). Here, h is the size of the element adjacent to the wall and $k > 1$ is a fixed number. The size of the elements are now h, kh, k^2h, k^3h,..., etc. This judicious construction of the grid produces accurate information in the vicinity of the wall.

As the marching in the downstream direction proceeds, the boundary layer grows which, in turn, requires an adjustment of the existing grid. We have adopted the following policy. The slope of the u velocity profile at the edge of the boundary layer is examined. If the slope exceeds a fixed tolerance, the grid is enlarged by the addition of several new nodes. Of course, the size of the new elements follow the geometric grid construction.

9. The significance of λ and the stability of the calculations

The theory of stability of a numerical scheme is well developed for the case of linear parabolic partial differential equations. This, however is not true for nonlinear equations. In the course of our calculations the following observations are made.

For a fixed k and h (the parameters involved in the costruction of the geometric grid), the relevant stability parameters are λ (the implicitness parameter introduced in (6.2)) and Δx (the stepsize). Once Δx is chosen, the parameter λ must lie in a neighborhood of $\lambda = 1$ in order to

insure stability. This neighborhood is enlarged as Δx is reduced. Given a particular stepsize, the attempt to obtain a meaningful apriori estimate of λ was not successful, so we had to appeal to a trial and error process.

In any event, the discussed finite element formulation is stable for laminar flows (regardless of the magnitude of λ) and it is only for turbulent calculations that one should be cautious about undesirable oscillations. The numerical results which are discussed in Section 10 are all obtained by setting $\lambda = 1$. We have not investigated the effect of λ on the accuracy of the calculations. An interesting observation is that increasing the parameter λ simply moves the onset of oscillations further downstream.

10. Numerical experiments

In this section, the finite element strategy is applied to several test cases. Specifically the following problems are considered,

(a) Uniform laminar flow past an isothermally heated flat plate.
(b) Uniform laminar flow past a flat plate with a step jump in the surface temperature.
(c) Uniform turbulent flow past an isothermally heated flat plate.
(d) Plane laminar stagnation flow impinging on an isothermally heated wall.
(e) Uniform laminar flow past an isothermally heated cylinder.

It will be seen that the finite element calculations agree with the analytical and the experimental results quite favorably. The cases (a), (b) and (d) are compared with the exact similarity solutions. In (c) we employ the 1/7 power law [7] and finally in (e) the experimental data is used.

The parameters which are common to all the above cases are listed below. All the values are in SI units.

ν_l = 0.1889E − 4,
ρ = 1.06,
Pr = 0.7072,
Pr_t = 0.9 for a turbulent flow,
α = 0.2671E − 4,
k_l = 0.2851E − 1,
c_p = 0.1007E + 4,
T_0 = 360°, except in (e),
T_∞ = 300°,
Δx = 0.01, except in (e),
L = 1, except in (e),
x_0 = 0.01, except in (e).

(a) *Uniform laminar flow past an isothermally heated flat plate.* Here the free stream velocity is chosen to be $U_\infty = 1$ which results in a Reynolds number of Re = 52938.

Both the slug distribution and the uniform distribution are used to simulate the initial temperature profile. We find that the former yields more accurate results (see Fig. 6). Initially 26 nodes across the layer are employed and at the final station, this is increased to 41. This increase is due to the growth of the boundary layer.

Figs. 5 and 6 are the local friction coefficient and Nusselt numbers. The agreement with the exact similarity solution is quite good.

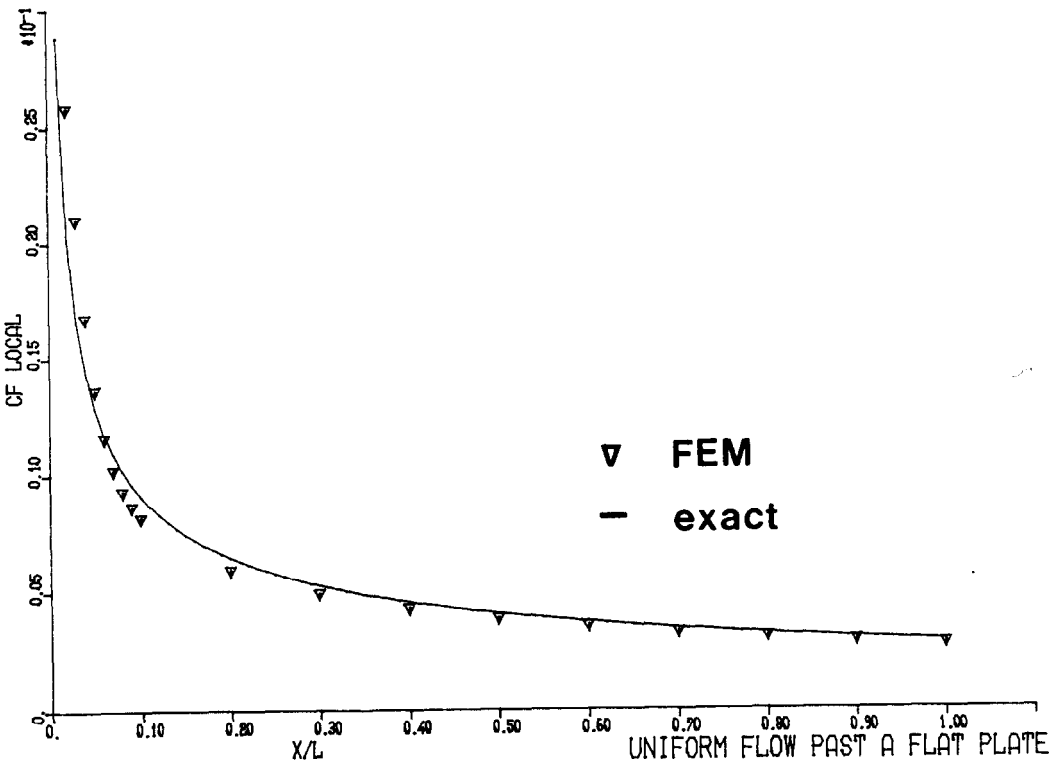
CF LOCAL
X/L
FEM
exact
UNIFORM FLOW PAST A FLAT PLATE

Fig. 5.

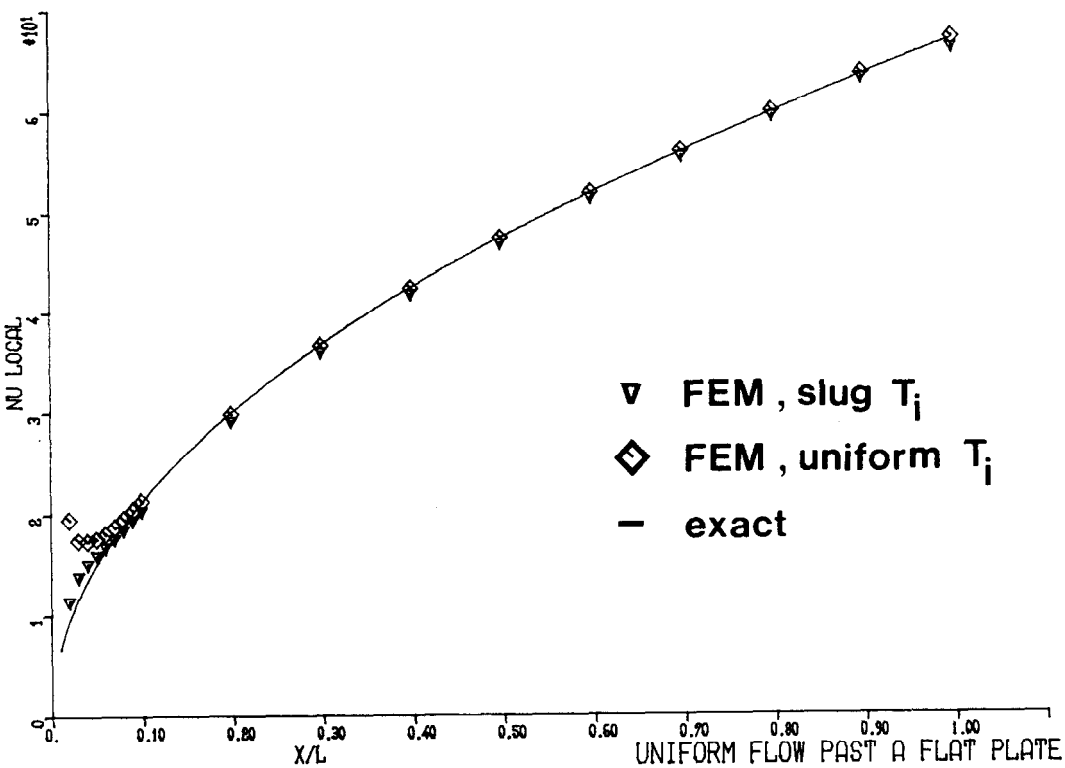
NU LOCAL
X/L
FEM , slug T_i
FEM , uniform T_i
exact
UNIFORM FLOW PAST A FLAT PLATE

Fig. 6.

(b) *Uniform laminar flow past a flat plate with a step jump in the surface temperature* [7]. The surface temperature is prescribed below

$$T_0 = \begin{cases} 300°, & 0 < x < 0.1, \\ 360°, & 0.1 < x < 1. \end{cases}$$

The free stream velocity and consequently the Reynolds number are as in (a). Thus, momentum calculation results are identical to the previous case whereas the local Nusselt number is different. Fig. 7 shows the Nusselt number obtained from two different sets of initial temperature profiles. Due to the better accuracy of the slug distribution, in the remaining cases only this distribution is prescribed. The comparison with the analytical solution is encouraging.

(c) *Uniform turbulent flow past an isothermally heated flat plate.* In this case, $U_\infty = 10$ which results in a higher Reynolds number of Re = 529381. The initial and final numbr of nodes are 15 and 45 respectively. The local friction coefficient and Stanton numbers are shown in Figs. 8 and 9. Clearly the calculation results agree quite well with 1/7 power law.

(d) *Plane laminar stagnation flow impinging on an isothermally heated wall.* The free stream velocity and Reynolds number are identical to (a). The initial and final number of nodes are 41. This is due to the fact that in a stagnation flow, the boundary layer thickness is constant. The local friction coefficient and Nusselt numbers are shown in Figs. 10 and 11 respectively.

(e) *Uniform laminar flow past an isothermally heated cylinder.* The initial point is assumed to be $x_0 = 0.0044$. The characteristic length and free stream velocity are taken as $L = 0.05$ and

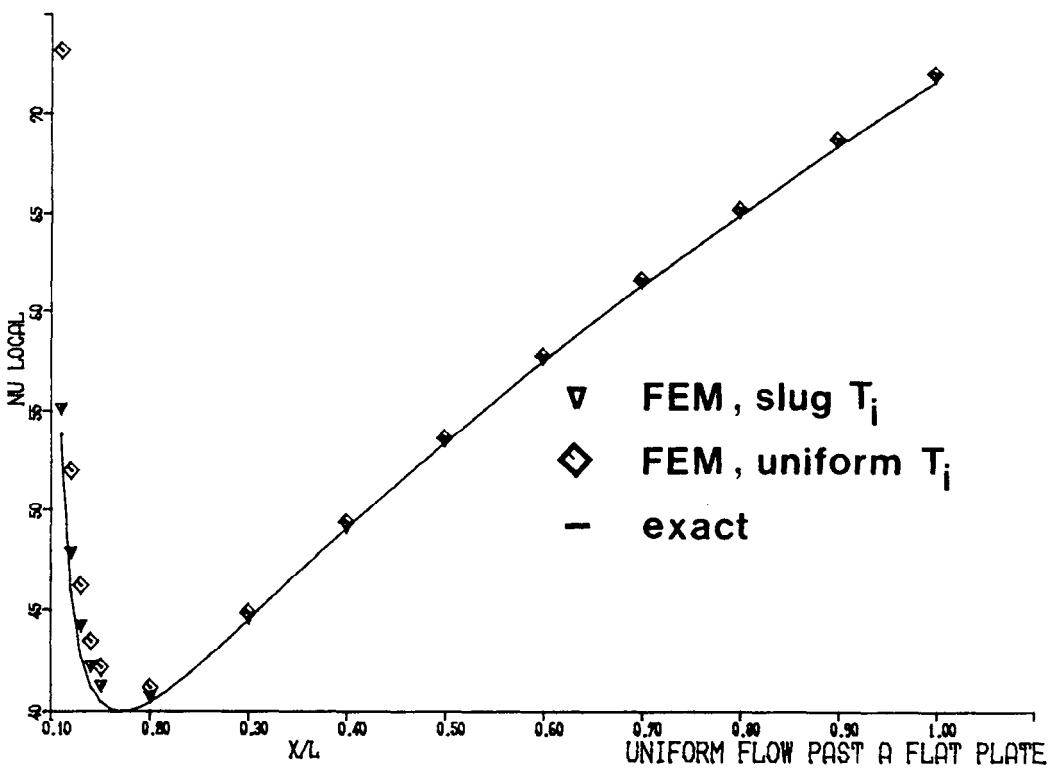

Fig. 7.

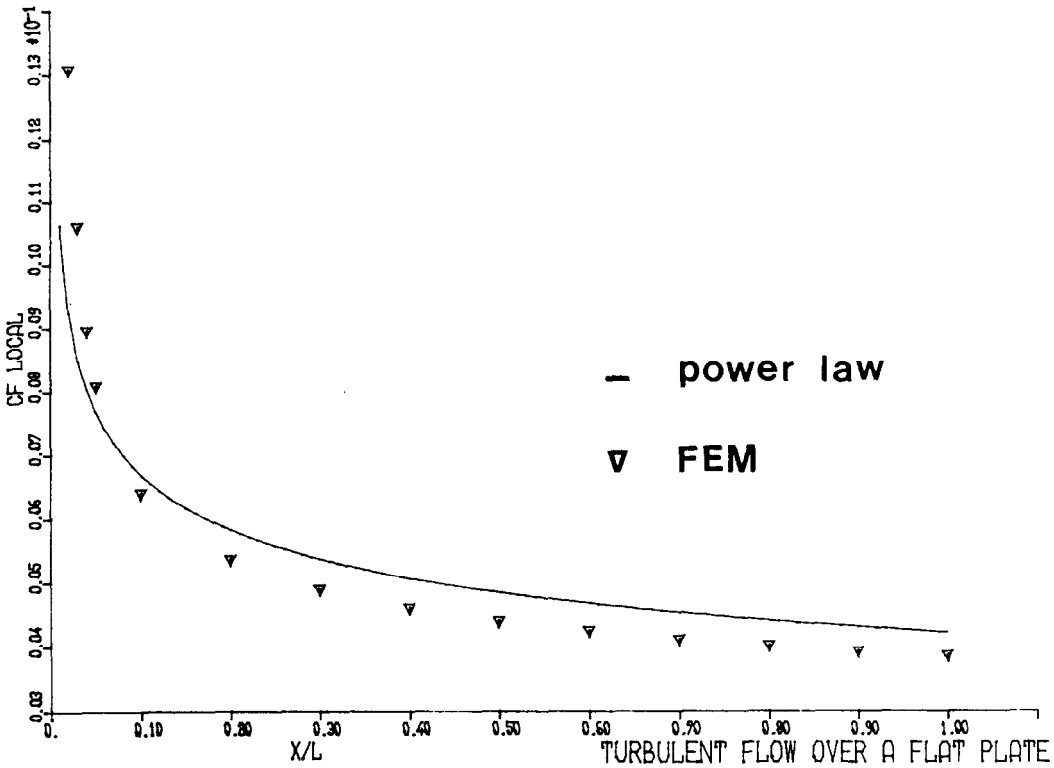
CF LOCAL
X/L
power law
FEM
TURBULENT FLOW OVER A FLAT PLATE

Fig. 8.

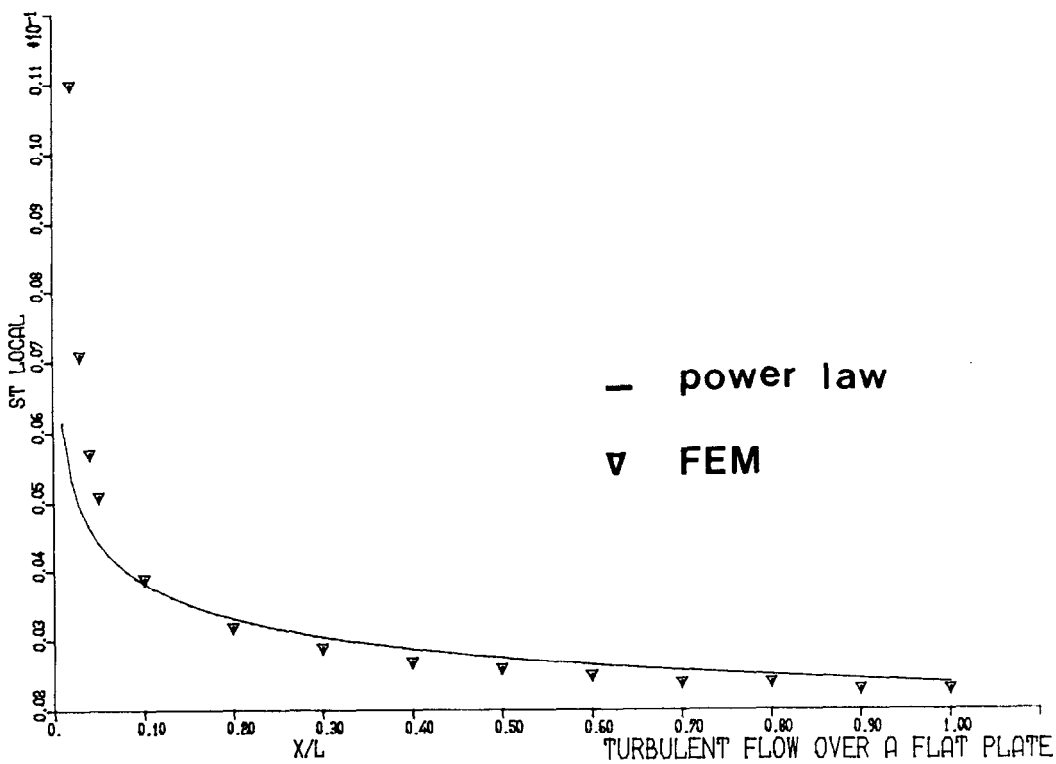
ST LOCAL
X/L
power law
FEM
TURBULENT FLOW OVER A FLAT PLATE

Fig. 9.

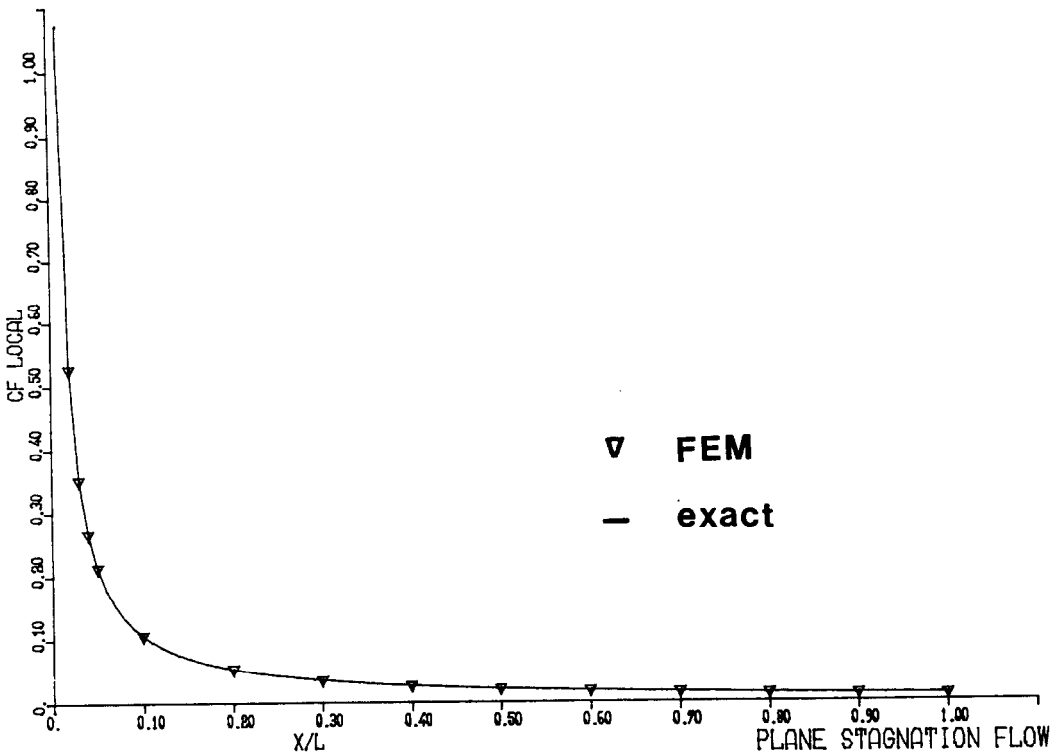
CF LOCAL
0.
0.10
0.20
0.30
0.40
0.50
0.60
0.70
0.80
0.90
1.00
X/L
FEM
exact
PLANE STAGNATION FLOW

Fig. 10.

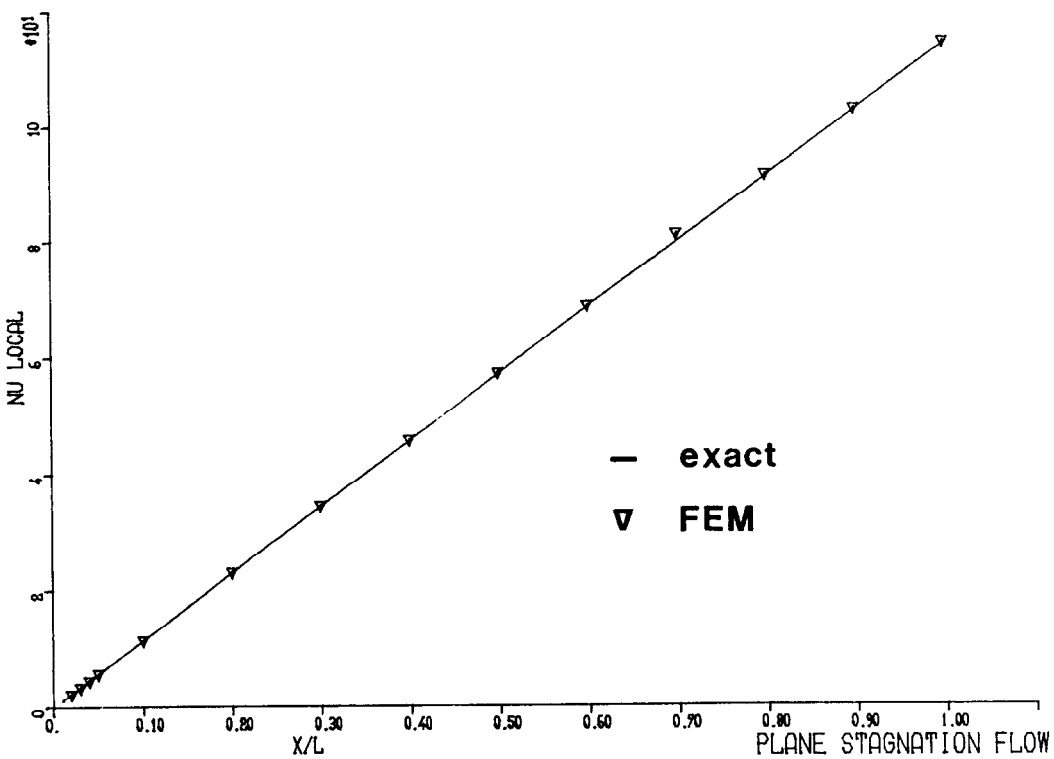
NU LOCAL
0
2
4
6
8
10
*10¹
0.
0.10
0.20
0.30
0.40
0.50
0.60
0.70
0.80
0.90
1.00
X/L
exact
FEM
PLANE STAGNATION FLOW

Fig. 11.

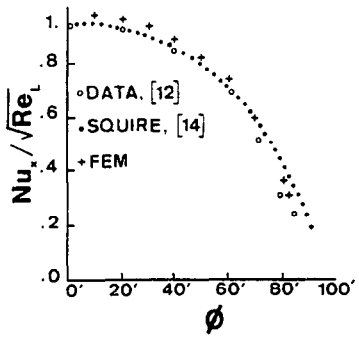

Fig. 12.

$U_\infty = 18.889$. Such a choice leads to a Reynolds number of $\mathrm{Re} = 50000$. The initial and final number of nodes are 10 and 11 respectively.

The data are due to Schmidt and Wenner [12] and were taken at a Reynolds number of 50000. The potential flow velocity is the formula of Sogin and Subramanian [13] which reads as

$$u_p = u_\infty \left[1.82\frac{x}{a} - 0.4\left(\frac{x}{a}\right)^3\right], \quad \phi = \frac{x}{a}.$$

This formula is based on a Reynolds number of 61000. For details see [16]. According to the above potential flow velocity, the separation occurs at roughly 85°. Fig. 12 shows the comparison between experimental results, the finite element calculations and a two parameter integral relation [14]. Clearly as the point of separation is approached, the discrepency with data becomes more pronounced.

11. Concluding remarks

The calculation results in the previous section show that the finite element method can accurately predict the development of incompressible thermal boundary layers. Although the problem considered is two-dimensional, there is no difficulty in extending the procedure to three dimensions.

Finite difference boundary layer codes, e.g., [2,3,5,11], have been in use for a long time and have performed quite well. The purpose of this article is to show that the finite element method compares favorably with other numerical techniques in the field of fluid dynamics.

As far as theoretical development is concerned, results such as those presented by Baker and Soliman in [1] are in great demand but at the same time difficult to obtain. One major difficulty is the nonlinearity of the fluid flow equations. In the context of boundary layer calculations, some heuristic arguments are given in [17].

The present paper has employed linear shape functions only. A different choice of the trial and test functions leads to collocation algorithm which is a particular finite element technique. The application of collocation to boundary layers is considered in [18].

Acknowledgment

The authors would like to thank the referee for his careful reading of the article and his constructive comments.

References

[1] A.J. Baker and M.O. Soliman, Accuracy and convergence of a finite element algorithm for turbulent boundary layer flow, *Comput. Meths. Appl. Mech. Engrg.* **28** (1981) 81–102.
[2] F.G. Blottner, Investigation of some finite difference techniques for solving the boundary layer equations, *Comput. Meths. Appl. Mech. Engrg.* **6** (1975) 1–30.
[3] P. Bradshaw, D.H. Ferris and N.P. Atwell, Calculation of boundary layer development using the turbulent energy equation, *J. Fluid Mech.* **28** (1967) 593–616.
[4] L.W.B. Browne and R.A. Antonia, Calculation of a turbulent boundary layer downstream of a step change in surface temperature, *J. Heat Transfer, ASME Trans.* **101** (1979) 144–150.
[5] T. Cebeci and A.M.O. Smith, *Analysis of Turbulent Boundary Layers* (Academic Press, New York, 1974).
[6] H.J. Herring and G.L. Mellor, A computer program to calculate incompressible laminar and turbulent boundary layer development, NASA CR-1564, 1970.
[7] W.M. Kays and M.E. Crawford, *Convective Heat and Mass Transfer* (McGraw-Hill, New York, 1980).
[8] B.E. Launder and D.B. Spalding, *Mathematical Models of Turbulence* (Academic Press, New York, 1972).
[9] P.P. Lynn, Least squares finite element analysis of laminar boundary layer flows, *Internat. J. Numer. Methods in Engrg.* **8** (1974) 865–876.
[10] P.M. Moretti and W.M. Kays, Heat transfer to a turbulent boundary layer with varying free stream and varying surface temperature—an experimental study, *Internat. J. Heat Mass Trans.* **8** (1965) 1187–1202.
[11] S.V. Patankar and D.B. Spalding, A finite difference procedure for solving the equations of two dimensional boundary layer, *Internat. J. Heat Mass Trans.* **10** (1967) 1389.
[12] E. Schmidt and K. Wenner, *Forsch. Ing.-Wes.*, **13** (1941) 612–614.
[13] H.H. Sogin and V.S. Subramanian, *J. Heat Trans.* **83** (1961) 483.
[14] H.B. Squire, RM-1986, Aeronautical Res. Council, London, 1942.
[15] E.R. Van Driest, On turbulent flow near a wall, *J. Aeron. Sci.* **23** (1956) 1007.
[16] F.M. White, *Viscous Fluid Flow* (McGraw-Hill, New York, 1974).
[17] N.G. Zamani, A finite element code for two dimensional, incompressible, laminar and turbulent boundary layer equations, Tech. Rept, Dominion Engineering Works, Montreal, 1982.
[18] N.G. Zamani, A collocation finite element method for integration of the boundary layer equations, *J. Appl. Math. and Comput.* (1984) to appear.